THE JOURNAL OF PHYSICAL CHEMISTRY C

Article

pubs.acs.org/JPCC

Effect of Posttreatment of Titania Mesoscopic Films by $TiCl_4$ in Solid-State Dye-Sensitized Solar Cells: A Time-Resolved Spectroscopy Study

Arianna Marchioro,[†,‡] Amalie Dualeh,[‡] Angela Punzi,[†,§] Michael Grätzel,[‡] and Jacques-E. Moser*[,†]

[†]Photochemical Dynamics Group and [‡]Laboratory for Photonics and Interfaces, Institute of Chemical Sciences and Engineering, École Polytechnique Fédérale de Lausanne, CH-1015 Lausanne, Switzerland

Supporting Information

ABSTRACT: Posttreatment of mesoporous titanium dioxide films by $TiCl_4$ solutions is commonly applied during the fabrication of solid-state dye-sensitized solar cells (ssDSCs), as this operation markedly improves the performance of the photovoltaic device. The effect of the posttreatment upon the charge carrier dynamics was scrutinized in an ssDSC aiming at unraveling its mechanism. Kinetic studies carried out using femtosecond and nanosecond transient absorption spectroscopies showed that a biphasic electron injection from the dye excited state is observed, for both treated and nontreated films, whose kinetics is not significantly affected by the surface modification step. However, hole injection in the hole transport material (HTM) spiro-OMeTAD and charge recombination were found to be markedly slower in $TiCl_4$-treated films. These findings are rationalized by a model describing the interaction at the interface between TiO_2, the dye-sensitizer, and spiro-OMeTAD. Rather than resulting from a modification of the energetics of the conduction band of the oxide, the effect of the $TiCl_4$ posttreatment appears to be associated with a subtle change of the film morphology. Results emphasize the importance of controlling the contact at the heterojunction between the HTM and the sensitized semiconductor oxide network.

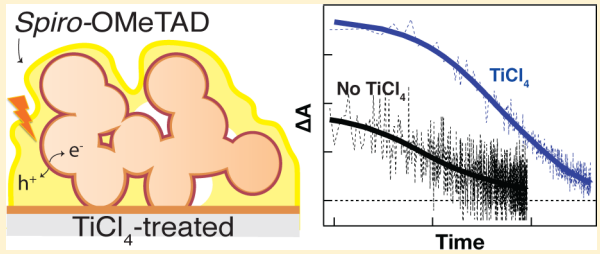

INTRODUCTION

Solid-state dye-sensitized solar cells (ssDSCs), first reported in 1998 by Bach et al.,[1] are a promising alternative to conventional dye-sensitized cells (DSCs), as they circumvent potential problems of spilling and corrosion related to liquid electrolytes. Nowadays, systems based on solid organic hole transporting materials (HTMs) in conjunction with molecular dye sensitizers reach 7.2% power conversion efficiency.[2] Compared to electrolyte-based DSCs with certified power conversion efficiencies of 12%,[3] there is still some room for performance improvement.

Under sunlight, the sensitizer, usually a carboxylated ruthenium(II) heteroleptic polypyridyl complex, undergoes several consecutive charge transfer processes: absorption of sunlight leads first to a metal-to-ligand charge transfer (MLCT) transition. Electron injection occurs then from the electronic excited state of the dye (S*) into the conduction band of a wide band gap oxide semiconductor such as TiO_2 (femtosecond to picosecond time scale) (eq 1). Finally, regeneration of the sensitizer is ensured by hole injection into the HTM (picosecond to nanosecond time frame) (eq 2). Undesirable back reactions can occur when electrons in the conduction band (e^-_{cb}) either recombine with some oxidized dye molecules (S^+), which did not inject holes sufficiently fast because of poor contact with the HTM, or directly with the oxidized HTM (eqs 3 and 4). These recombination reactions are usually slower than forward electron transfer processes and take place in the microsecond time scale. Reductive quenching of the dye's excited state by the HTM is also a pathway that needs in principle to be addressed in these systems (eq 5).[4]

$$S^*|TiO_2 \rightarrow S^+|TiO_2 + e^-_{cb} \quad (1)$$

$$S^+|TiO_2 + HTM \rightarrow S|TiO_2 + HTM^+ \quad (2)$$

$$e^-_{cb} + S^+ \rightarrow S \quad (3)$$

$$e^-_{cb} + HTM^+ \rightarrow HTM \quad (4)$$

$$S^*|TiO_2 + HTM \rightarrow S^-|TiO_2 + HTM^+ \quad (5)$$

As the DSC working principle relies on kinetic competition between forward charge transfer and recombination processes, it is crucial to gain deeper insight into the study of carrier dynamics, namely the kinetics of holes and electrons following light excitation, in order to fully understand the origin of the limitations in ssDSCs. Despite a large research effort aimed at improving the efficiency of these solid-state devices, up to now only few studies concerning the mechanistic processes occurring in the system have been reported.

Received: October 3, 2012
Revised: November 28, 2012
Published: November 30, 2012

dx.doi.org/10.1021/jp309799u | J. Phys. Chem. C 2012, 116, 26721−26727

The hole mobility and the pore wetting/filling appear to be key parameters controlling charge separation efficiency. As the accumulation of holes at the interface would lead to increased recombination and prevent further hole injection from the dye, a good hole mobility in the HTM is needed, and so far this is practically achieved by the use of various dopants.[2,5−7] The other main issue is related to the contact between adsorbed dye molecules and the hole transport material:[8−10] In the case of inhomogeneous and incomplete contact, the hole will not be efficiently extracted and transported. These two parameters are interconnected and related to the way the HTM has infiltrated the TiO_2 mesoporous structure; thus they strongly depend on the morphology and thickness of the film. The way the TiO_2 film is prepared must then be carefully considered. Recently, new TiO_2 architectures have been tested to maximize the penetration of the HTM, and this field is currently under investigation.[11] On the other hand, posttreatment of the surface of mesoporous titania films constituted of sintered spherical nanoparticles by bath deposition of TiO_2 from $TiCl_4$ aqueous solutions is routinely done in DSC fabrication, as it markedly improves their photovoltaic efficiency and decreases recombination.[12,13] This surface posttreatment of TiO_2 nanocrystalline anodes is indeed expected to increase the necking between nanoparticles and fill possible cracks in the film.[14] The main effect observed in liquid DSCs is an enhancement of the photocurrent associated with a downward shift of the conduction band edge energy level. Sommeling et al. reported a complete work hypothesizing an effect of $TiCl_4$ on electron injection after ruling out a possible implication in electron transport and improved dye loading.[12] At this point, however, no systematic study on the effect of $TiCl_4$ treatment on solid-state devices has been performed. As the wetting of the surface with the HTM is critical for these devices, it is even more important to understand how surface treatments influence the morphology of the semiconductor film and affect the dynamics of electron transfer processes at the interface.

Here we report on the effect of $TiCl_4$ treatment upon the kinetics of charge transfer in ssDSCs studied by time-resolved transient absorption spectroscopy (TAS). By monitoring transient signals over a wide time range spanning from femtoseconds to milliseconds, TAS represents a powerful method to investigate the mechanistic processes occurring in a photovoltaic device. Charge separation and charge recombination pathways in ssDSCs were examined in the presence or absence of $TiCl_4$ posttreatment. Here, we show that adding this specific fabrication step affects the kinetics of processes in solar cells drastically, and that these changes are related to one of the bottleneck parameters of ssDSCs, i.e., the contact between the dye and the HTM spiro-OMeTAD. First, we investigated the impact of $TiCl_4$ treatment on electron injection dynamics. Then, the effect on hole injection of different $TiCl_4$ treatment procedures was determined systematically. Besides the hole injection reaction (picosecond to nanosecond time scale), the competing back reaction of conduction band electrons (e^-_{cb}) with the oxidized form of the HTM (microsecond time scale) in treated and nontreated films was also investigated in order to provide a complete picture of the kinetic competition in the system.

EXPERIMENTAL SECTION

Sample Preparation. Nanocrystalline mesoporous 2.0−2.5 μm thick TiO_2 films were prepared by screen-printing an aqueous paste onto glass microscope slides and sintering at a temperature of 500 °C. The samples treated by $TiCl_4$ were prepared as follows: the TiO_2 films were immersed in the dark in 20 mM aqueous titanium tetrachloride solution at either 70 °C for 30 min or room temperature (RT) for 6 h, prior to sintering at 500 °C for 30 min. These two treatments influenced the morphology of the initially prepared mesoporous TiO_2 film, although not in a similar way. Scanning electron microscopic (SEM) pictures of TiO_2 compact films, which were not used for the kinetic studies, are presented in the Supporting Information (Figure S6) and show how 70 °C treatment formed a conformal layer over the TiO_2 sintered nanoparticles, while RT treatment formed an additional layer including the nucleation of small islands.

Z907 complex (*cis*-bis(isothiocyanato)(2,2′-bipyridyl-4,4′-dicarboxylato)(4,4′-dinonyl-2′-bipyridyl)Ru^{II}) was used as a dye sensitizer in this study.[15] Sensitization of mesoporous TiO_2 was achieved by immersing the films overnight in a 0.3 mM Z907 solution in a mixture (1:1) of *tert*-BuOH and MeCN solvents. Samples infiltrated by spiro-OMeTAD HTM were prepared in an argon glovebox following a standard procedure to avoid any oxygen or moisture contact. Spiro-OMeTAD (Merck, KGaA, used as received) was dissolved in 400 μL of chlorobenzene at a concentration of 180 mg/mL by heating for 30 min at 60 °C. Lithium bis(trifluoromethylsulfonyl)imide (LiTFSI) and 4-*tert*-butylpyridine (tBP) were added as follows: tBP was purified before use and 7 μL of this compound was added to the chlorobenzene solution to yield a concentration of 0.12 M tBP. Seventeen milligrams of LiTFSi was predissolved in 100 μL of acetonitrile, and 15 μL of this solution was added to the chlorobenzene solution to yield a concentration of 0.02 M LiTFSI. A 40 μL volume of spiro-OMeTAD solution was deposited onto the sensitized substrates and allowed to infiltrate for 30 s in order to maximize the penetration of the HTM prior to spin-coating for 30 s at 2000 rpm. After overnight evaporation of residual chlorobenzene, cells were sealed with Surlyn (DuPont) cast polymer film and cover glass. Reference samples, containing no hole transport material, were covered with a solution of propylene carbonate with LiTFSI and tBP dissolved at the same concentration as the solution prepared for spiro-OMeTAD-infiltrated samples.

Nanosecond Flash Photolysis. Transmission-mode TAS experiments were conducted using a frequency-tripled, Q-switched Nd:YAG laser (Continuum, 20 Hz repetition rate) pumping an optical parametric oscillator (OPO) (GWU-355). The output wavelength of the OPO was tuned at λ = 590 nm (7 ns pulse duration). The sample was set at a 60° angle to the excitation laser beam. The excitation light beam was attenuated to a fluence at the sample of less than 40 $\mu J/cm^2$·pulse in order to inject less than two electrons per nanoparticle on the average per pulse and thus ensure that no significant shift in the TiO_2 Fermi level occurs as a result of a higher injected electron population. The CW probe light from a Xe arc lamp was passed through various optical elements, the sample, and a monochromator (λ_{probe} = 1000 nm) before being detected by a fast photodiode. Averaging over at least 1000 laser shots was necessary to get satisfactory signal/noise ratios.

Femtosecond Transient Absorption Spectroscopy (TAS). The setup is described in detail elsewehere.[16] Briefly, a Ti:sapphire amplified femtosecond laser (CPA-2001, Clark-MXR) was used as a source. The laser had 1 kHz repetition frequency, with typical pulse energy of 950 μJ at a fundamental wavelength of 775 nm, and pulse duration of 140 fs. Half the source intensity was used for pumping two noncollinear phase-

matched optical parametric amplifiers (NOPAs), allowing for the generation of monochromatic pump and probe beams. At 590 nm pump wavelength, a typical energy of 8 μJ/pulse was obtained. The probe NOPA allowed the generation of a near-IR beam, with λ_{probe} = 840 nm and pulse energy of 1.5 μJ. The spectral profile of the pulses was measured using a dual-channel CCD spectrometer (S2000, Ocean Optics). The output pulses of the NOPAs were compressed by pairs of SF10 prisms down to sub-50 fs durations. The temporal profile of the pulses was determined using an autocorrelator (APE PulseCheck 15 Short Pulse). The relative path length between the two beams was changed with a delay line, alternatively on the pump or on the probe pulse. The translation stage (M521.PD, Physik Instrumente) allowed time steps of 10 fs and generated delays up to 2 ns. The pump beam was chopped at half the repetition frequency of the pulsed laser source. The change in transmittance of the sample, i.e., change in intensity of the probe beam, was measured by a photodiode (Nirvana detector, New Focus, Model 2007) placed after the sample and protected by cutoff filters to avoid any scattered light from the pump. The low-amplitude signal was extracted by a lock-in amplifier (SR-830, Stanford Research) referenced to the chopper. To ensure isotropic excitation of the sample, the pump polarization was set at the magic angle (54.7°) relative to the probe pulse with a $\lambda/2$ waveplate. The typical fluence of the pump on the sample was low (230 μJ/cm^2·pulse; this should correspond, with a transmittance of 0.66 of the sample, to approximately eight injected electrons per TiO_2 nanoparticle). A lens allowed tuning the size of the pump beam before the sample to both decrease the fluence and allow for complete overlap of the probed spot area. Temporal overlap between the pump and probe pulses at the sample position was measured with a Kerr gating technique and gave a typical instrument response function (IRF) of 120 fs.

RESULTS

Femtosecond and nanosecond TAS measurements were performed on samples prepared with and without $TiCl_4$ treatment. Z907 dye was used throughout the study. Dye photoexcitation was carried out at 590 nm, and the dye oxidized state's transient absorption was probed at 840 nm. The choice of the probe wavelength is explained in the Supporting Information in more detail. Spectra of Z907/TiO_2 films and Z907 + spiro-OMeTAD/TiO_2 films are presented in the Supporting Information (Figures S3, S5).

Electron Injection Dynamics. At first, the influence of $TiCl_4$ treatment on electron injection dynamics from Z907 was monitored. Films of Z907/TiO_2 were prepared as described in the Experimental Section, but no spiro-OMeTAD was deposited. Electron injection has been reported to take place in the femtosecond time scale, provided that dye adsorption on the surface is performed under certain conditions.[17−20] TAS measurements over a time span of 1 or 2 ns were conducted on Z907 sensitized TiO_2 samples with and without $TiCl_4$ treatment. The samples were covered with propylene carbonate (PC) as an inert solvent. Measurements were performed both with neat PC and with a solution of PC containing LiTFSI and tBP at the same concentrations used for the preparation of the spiro-OMeTAD solution, and no noticeable difference was observed within the two sets of samples. No difference was also observed between different $TiCl_4$ treatments (70 °C treatment or RT treatment). At 840 nm, the observed signal corresponds mainly to the formation of the dye oxidized state (S^+) by electron injection in the TiO_2 as explained in the Supporting Information. This dye oxidized state, in the absence of a redox mediator, has a lifetime of a few hundreds of microseconds. Thus, on the time scale of the experiment, only the rise of the S^+ species signal can be detected, as can be seen in Figure 1.

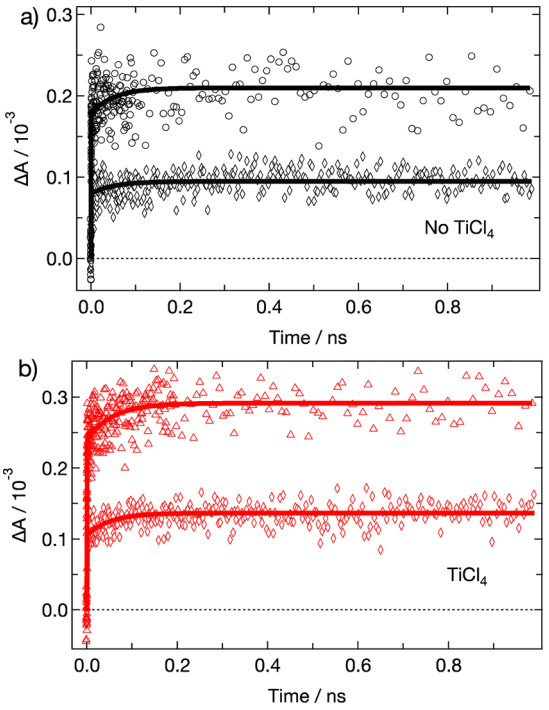

Figure 1. Time course of the transient absorption measured at 840 nm of samples following femtosecond pulsed excitation at 590 nm. Signals mainly reflect the kinetics of appearance of the dye oxidized state S^+ and, therefore, of the electron injection process. (a) Z907/nontreated TiO_2. Black circles: sample measured under an excitation fluence of 230 μJ/cm^2. Black diamonds: different sample measured at half the fluence. (b) Z907/$TiCl_4$-treated TiO_2 at 70 °C. Red triangles: sample measured under an excitation fluence of 230 μJ/cm^2. Red diamonds: different sample measured at half the fluence. Data were fitted with an analytical convolution function of a Gaussian instrument response and two exponential rises (solid lines).

Electron injection in nontreated films was found to take place predominantly in a sub-50 fs time scale, with a small slower picosecond component (15%, 50 ps) being consistent with previous results.[19] A similar biphasic behavior was found in the case of the treated films, with a 60 ps component accounting for 20% of the total signal. This is also consistent with findings of Tiwana et al., who observed by terahertz measurements a biphasic charge injection with a 50−70 ps component and no noticeable difference in charge injection for treated and nontreated samples.[21] Samples were also measured with different fluences in order to ensure that the dynamics of electron injection is independent of the pump energy.

Hole Injection Dynamics. The dye oxidized state S^+ signal of samples filled with spiro-OMeTAD HTM was monitored by probing its optical absorption at 840 nm as explained in the Supporting Information. Typical transients are shown in Figure 2. The regeneration of the oxidized dye (eq 2) was expected to occur on the picosecond to nanosecond time scale,[22] and indeed a decrease in the dye oxidized signal can be observed over a range of 2 ns. At the probing wavelength of 840 nm, the observed signal includes contributions of the excited state, the

dx.doi.org/10.1021/jp309799u | J. Phys. Chem. C 2012, 116, 26721−26727

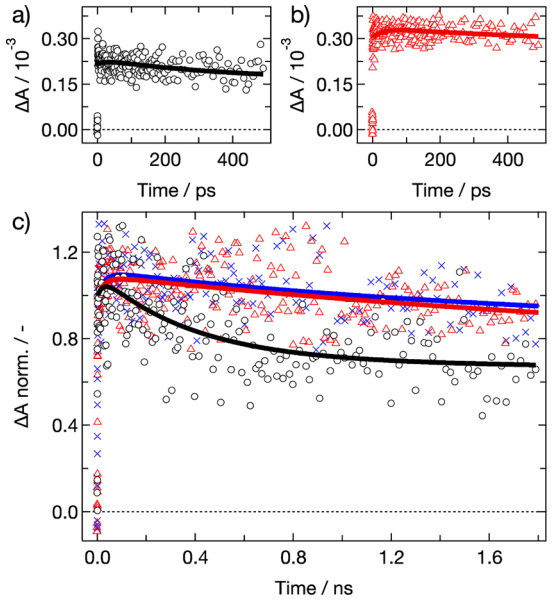

Figure 2. Hole injection dynamics probed at 840 nm following 590 nm femtosecond pulsed excitation of dye-sensitized TiO_2 films. (a) Z907 + spiro-OMeTAD/nontreated TiO_2. (b) Z907 + spiro-OMeTAD/$TiCl_4$-treated TiO_2 at 70 °C. (c) Normalized absorbance changes of (a) (black dots) and (b) (red triangles) are plotted together for direct comparison. Data obtained for a sample made of Z907 + spiro-OMeTAD/$TiCl_4$-treated TiO_2 at RT are also shown (blue crosses).

oxidized state, the oxidized HTM, and conduction band electrons. Thus, it is hardly possible to extract quantitative kinetic information without a precise description of the time evolution of each species. A detailed model describing the time-dependent contribution of each species, weighted by the corresponding relative extinction coefficient, is described in the Supporting Information. The model considers two types of population of oxidized dye, S_A^+ and S_B^+, corresponding respectively to a dye population A, where molecules are adsorbed in direct contact with the HTM, and to a portion B of dye molecules not in direct contact with the HTM, and for which holes have to be transferred by lateral hopping until they reach the HTM.[23,24] The fit equation derived with the model allowed obtaining quantitative values for the initial volumic concentrations on the probed spot and time constants for each species (respectively $S_{A,0}^+$ and k_A, and $S_{B,0}^+$ and k_B) separated from the contributions of all the other absorbing species. Figure 2a,c shows transient absorption signals recorded in similar conditions with samples prepared with nontreated films. The fast component, with $k_A = 2.6 \times 10^9$ s^{-1} ($\tau_A = 380$ ps), accounts for 52% of the total oxidized dye concentration, while the slow component $k_B = 2.6 \times 10^7$ s^{-1} ($\tau_B = 38$ ns) accounts for 48% of the total oxidized dye concentration. Residues for all fits are presented in Supporting Information (Figure S2).

Hole Injection in $TiCl_4$-Treated Samples. Samples with different types of $TiCl_4$ treatment were prepared, and hole injection dynamics was measured. Decrease of the dye oxidized state signal was observed to be slower in the case of $TiCl_4$ treatment than with nontreated films (Figure 2b,c). Similar to the previous case, the derived model provided an estimation of the proportion of the population A with respect to the population B without any contribution from the HTM absorption, the electrons, or the dye excited state. The fit equation derived also takes into account the small differences observed in the case of electron injection. Consequently, it can be unambiguously determined if the observed decrease results from slower electron injection or if it is solely related to an effect due to different surface morphology. For a sample prepared with a $TiCl_4$-treated film, a fast component is still observable, $k_A = 1.4 \times 10^9$ s^{-1} ($\tau_A = 710$ ps), but this accounts for only 14% of the total oxidized dye concentration, while the slow component with $k_B = 5 \times 10^7$ s^{-1} accounts for 86% of the total oxidized dye concentration. This shows that the hole injection is markedly delayed when $TiCl_4$ treatment is implemented.

Hole Injection with Different $TiCl_4$ Treatments. Empirical optimization of $TiCl_4$ treatment in our laboratory suggested that varying the conditions of the surface treatment leads to a change in the morphology of the film. In order to compare the effect of distinct types of $TiCl_4$ treatments and the related morphology of the TiO_2 films on the hole injection, samples with a different $TiCl_4$ treatment, done at 25 °C for 6 h, were tested. Electron injection on a Z907 sensitized TiO_2 film was first tested to extract the parameters needed for the fitting procedure, and it was found to be very similar to the previous 70 °C $TiCl_4$ treatment. For samples Z907 + spiro-OMeTAD/$TiCl_4$-treated TiO_2 at RT, no noticeable difference could be observed for hole injection (Figure 2c) within the resolution of measurements. Fast component with $k_A = 8.1 \times 10^8$ s^{-1} ($\tau_B = 1.2$ ns) and the slower one with $k_B = 5 \times 10^7$ s^{-1} accounted for 11 and 89% of the total oxidized dye concentration, respectively.

Charge Recombination. Charge recombination of oxidized spiro-OMeTAD with electrons in the TiO_2 conduction band is in the microsecond time scale and can be monitored by the flash photolysis technique. Measurements were performed on Z907 + spiro-OMeTAD/TiO_2 samples prepared with and without $TiCl_4$ treatment. The dye was excited at 590 nm, and the spiro-OMeTAD oxidized state (HTM^+) was probed at 1000 nm, where the oxidized spiro-OMeTAD state absorbs,[25] with only a small contribution of conduction band electrons. This particular wavelength was chosen to exclude the contribution to the signal from possible remaining oxidized dye molecules. The decay of the absorption of HTM^+ displayed in Figure 3 reflects the recombination of spiro-OMeTAD oxidized state species with injected conduction band electrons (eq 4). A simple single exponential was not able to fit the decay kinetics. As excitation fluences were carefully limited to ensure that less than two electrons are injected per nanoparticle at a time, the observed complex kinetics could well indicate a kinetically inhomogeneous recombination mechanism. Non-treated films ($k_1 = 1.5 \times 10^5$ s^{-1} and $k_2 = 2.6 \times 10^4$ s^{-1}) exhibit a faster recombination than samples having been treated with the two different types of $TiCl_4$ treatment ($k_1 = 2.8 \times 10^4$ s^{-1} and $k_2 = 4.3 \times 10^3$ s^{-1} for 70 °C treatment and $k_1 = 4.2 \times 10^4$ s^{-1} and $k_2 = 7.8 \times 10^3$ s^{-1} for RT treatment). In order to exclude variation of the recombination rate due to a shift in the Fermi level caused by an increased dye loading and consequently an increased number of injected electrons per particle, the dye loading was determined by dye desorption experiments (refer to the Supporting Information). As already reported by Sommeling et al.,[12] the measured adsorbed dye surface concentration was found to be practically constant (with changes of the order of 4%). The difference observed between recombination rates cannot be ascribed, thus, to a different density of injected electrons.

dx.doi.org/10.1021/jp309799u | J. Phys. Chem. C 2012, 116, 26721−26727

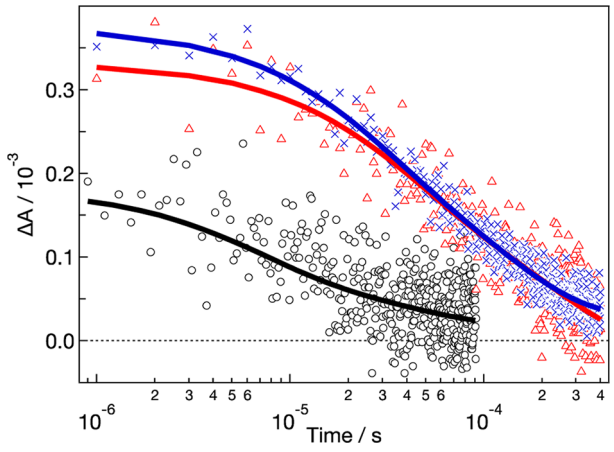

Figure 3. Charge recombination dynamics monitored at 1000 nm following excitation at 590 nm. Black circles represent Z907 + spiro-OMeTAD/nontreated TiO_2, red triangles represent Z907 + spiro-OMeTAD/$TiCl_4$-treated TiO_2 at 70 °C, and blue crosses represent Z907 + spiro-OMeTAD/$TiCl_4$-treated TiO_2 at RT. Experimental data points were fitted by double exponential decays (solid lines).

DISCUSSION

From the side of electron injection dynamics, this work confirms what was already observed using different techniques.[13,21] No marked difference is observable in the kinetics of electron injection that could be ascribed to the surface treatment. Furthermore, we cannot conclude on an effect of the treatment on the density of states of TiO_2. Here, the main interest of measuring electron injection is to determine a value for the biphasic injection to use as a parameter in the model developed for the hole injection.

Regarding hole injection, femtosecond TAS studies on ssDSCs were reported by Bach et al.[22] They investigated the process of hole injection by monitoring the bleaching of the dye and the appearance of the oxidized state of the spiro-OMeTAD, corresponding to the hole injection from the dye to the HTM. As one of the main issues with ssDSCs is partial pore filling that prevents part of the dye molecules from being in direct contact with the HTM, then monitoring the signal of oxidized dye, instead of the one from oxidized spiro-OMeTAD, gives a direct measure of the fraction of the isolated dye molecules not in contact with the HTM, which are consequently not regenerated. On the other hand, when probing the appearance of oxidized spiro-OMeTAD, this information is missing and may underestimate the fact that part of the dye molecules in a segregated zone, not in contact with spiro-OMeTAD, will follow completely different kinetics. As discussed above, preliminary studies on hole injection in the absence of any $TiCl_4$ treatment showed that the dye oxidized state could be monitored at 840 nm with little contribution from the spiro-OMeTAD oxidized state—thus leading to the choice of this particular probe wavelength for the reported work.

In ssDSCs using spiro-OMeTAD, hole injection is a one-electron-transfer process, unlike the case of liquid DSCs based on the I_3^-/I^- redox couple, where the oxidation of iodide implies a two-electron exchange.[7] Hole injection in HTM is, thus, expected to be fast, and indeed, the kinetic of dye regeneration is observed to take place in the picosecond to nanosecond time scale. The experiment showed that 50% of the dye is regenerated in a time scale of a few hundreds of picoseconds, while the other half of unregenerated dye is still present after 2 ns. From extrapolation, the totality of the dye should be regenerated after a few tens of nanoseconds. This observation is in agreement with Bach's studies in 1999, where the appearance of the oxidized state of spiro-OMeTAD was monitored, and it was concluded that the multiexponential kinetics arises from a distribution of separation distances between dye and HTM molecules.[22] This is a further indication that with optimized conditions of spiro-OMeTAD deposition (spin-coating, 180 mg/mL, 65% pore filling fraction), nearly all dye molecules are able to transfer their hole to spiro-OMeTAD, via direct contact or via lateral hole hopping. In a further study by the first author,[26] the effect of the pore filling fraction (PFF) on hole injection was investigated, showing that, between 25% PFF and 65% PFF, the regeneration increases with increasing PFF. This confirms a direct mechanism of hole injection for dye directly in contact with spiro-OMeTAD, while some holes have to move laterally in order to attain the next spiro-OMeTAD molecule, thus explaining the slower part of the signal.

Having established the mechanism of hole injection in the absence of $TiCl_4$ treatment, it was then possible to study the effect of $TiCl_4$ treatment on the same hole injection process. As pointed out by the results presented in Figure 2, hole injection is drastically slowed down by $TiCl_4$ treatment. A plausible hypothesis to explain this effect comes from a change in the morphology of the film observed as a result of a different necking between the particles, changing the pore size and the porosity. SEM pictures of the TiO_2 compact underlayer prepared following the same type of $TiCl_4$ treatment as the one applied to the mesoporous TiO_2 film are presented in the Supporting Information (Figure S6) and show indeed that the $TiCl_4$ bath induces a surface modification with deposition of additional material. In this sense, the penetration and/or wetting of the surface with spiro-OMeTAD could be more difficult after modification of the TiO_2 surface. This hypothesis is further supported by measurements carried out in the microsecond time scale, where recombination of e^-_{cb} with oxidized spiro-OMeTAD is monitored. Charge recombination between injected electrons and spiro-OMeTAD shows a 10-fold decrease of rate constants for treated samples with respect to nontreated ones, for both the 70 °C treatment and the RT treatment. This global decrease in both the hole injection and charge recombination process rates could be well explained by a different penetration of spiro-OMeTAD into the pores and a different wetting of the surface, slowing down the two competing reactions. As the overall effect of $TiCl_4$ treatment on complete cells is a general increase in their efficiency, it is safe to assume that the decrease in hole injection kinetics is not as crucial for the system as the decrease in charge recombination kinetics. Increasing the recombination time constant for this unwanted back reaction markedly improves the performance of the system, and these measurements confirm that a major effort has to be invested in trying to minimize this loss pathway. Recent studies have shown evidence for differences in recombination kinetics for different types of TiO_2 facets.[27] Looking from a molecular picture, it is then worth noting that if the TiO_2 local facet and orientation of dye molecules at the surface is a parameter that has to be taken into account. This could well explain the difference observed in recombination kinetics and hole injection, as the contact with the oxidized hole transport material and the lateral hopping between dye molecules is most likely altered.

When comparing the two different $TiCl_4$ treatments (at 70 °C and RT) on picosecond and microsecond time scales, the

dx.doi.org/10.1021/jp309799u | J. Phys. Chem. C 2012, 116, 26721−26727

following observation can be made: independently of which $TiCl_4$ treatment has been performed, hole injection is delayed in the same way with respect to a nontreated sample. As suggested by previous studies on the influence of PFF on the hole injection,[26] a noticeable difference in hole injection kinetics can be resolved only if the difference in PFF is greater than 10−20%. For small variations in PFF, as is assumed to be the case for samples prepared with the different $TiCl_4$ deposition methods, the change in hole injection dynamics must be too small to be observed within the resolution of our experiment.

While the effect of $TiCl_4$ treatment appears to be mitigated from the side of electron injection and goes in an opposite direction from what is expected for a performing cell regarding hole injection, the case of charge recombination shows a drastic change. Interestingly, the recombination of electrons and spiro-OMeTAD seems to be faster than the recombination of the electrons with the dye itself (usually a few hundreds of microseconds). This could be an indication that spiro-OMeTAD contacts directly the surface in some parts of the pore leading to a preferential channel for recombination. Further studies are being conducted to address these issues.

CONCLUSION

In conclusion, our study has focused on the effect of $TiCl_4$ treatment on both mechanisms of charge separation and charge recombination. TAS spectra of electron injection, hole injection, and charge recombination have been recorded, and a specific model was developed in order to treat the data obtained for hole injection from the oxidized dye to the HTM. This model allowed separating the contribution from the electrons, the oxidized HTM species, and dye molecules that absorb in the same region of the spectrum. Our findings show that the kinetics of electron injection is not significantly affected by $TiCl_4$ treatment. Hence, the beneficial effect of the posttreatment of the mesoscopic film on the performances of ssDSC devices cannot be attributed to a modification of the energetics of the conduction band of titania. By contrast, hole injection was found to be retarded by $TiCl_4$ treatment. This kinetic change was related to a different penetration/wetting of the pores by the HTM when deposited out of solution. The most striking effect of the surface treatment was found to be on charge recombination. These findings are in good agreement with previous studies that already concluded that the effect of $TiCl_4$ treatment in liquid cells was mostly affecting charge recombination. Charge recombination in solid devices being a one-electron process, it is likely to compete efficiently with the overall charge separation. This work underlines the importance of controlling charge recombination with the HTM in order to improve photovoltaic device performance.

ASSOCIATED CONTENT

Supporting Information

Model used to fit the data, residuals of the fits, absorption spectra, and SEM pictures. This material is available free of charge via the Internet at http://pubs.acs.org.

AUTHOR INFORMATION

Corresponding Author

*E-mail: je.moser@epfl.ch.

Present Address

[§]Hach Lange GmbH, Rte de Compois 6, CH-1222 Vésenaz, Switzerland.

Notes

The authors declare no competing financial interest.

ACKNOWLEDGMENTS

Financial support of this work by the Swiss National Science Foundation (SNF) through Grant 200020_134856 and the NCCR-MUST program is gratefully acknowledged. A.D. acknowledges financial support by EU FP7 project "ORION" Grant Agreement No. NMP-229036. The authors thank Dr. P. Infelta for his help in developing the mathematical model used to fit the data, Dr. S. M. Zakeeruddin for providing the Z907 dye, P. Comte for the preparation of TiO_2 nanoparticles, and Dr. F. Le Formal for the SEM pictures.

REFERENCES

(1) Bach, U.; Lupo, D.; Comte, P.; Moser, J.-E.; Weissörtel, F.; Salbeck, H.; Speitzert, H.; Grätzel, M. *Nature* **1998**, *395*, 583−584.
(2) Burschka, J.; Dualeh, A.; Kessler, F.; Baranoff, E.; Cevey-Ha, N.-L.; Yi, C.; Nazeeruddin, M. K.; Grätzel, M. *J. Am. Chem. Soc.* **2011**, *133*, 18042−18045.
(3) Yella, A.; Lee, H. W.; Tsao, H. N.; Yi, C.; Chandiran, A. K.; Nazeeruddin, M. K.; Diau, E. W. G.; Yeh, C. Y.; Zakeeruddin, S. M.; Grätzel, M. *Science* **2011**, *334*, 629−634.
(4) Wang, P.; Wenger, B.; Humphry-Baker, R.; Moser, J.-E.; Teuscher, J.; Kantlehner, W.; Mezger, J.; Stoyanov, E. V.; Zakeeruddin, S. M.; Grätzel, M. *J. Am. Chem. Soc.* **2005**, *127*, 6850−6856.
(5) Snaith, H. J.; Grätzel, M. *Appl. Phys. Lett.* **2006**, *89*, 262114-1−262114-3.
(6) Cappel, U. B.; Daeneke, T.; Bach, U. *Nano Lett.* **2012**, *12*, 4925−4931.
(7) Snaith, H. In *Dye-Sensitized Solar Cells*; Kalyanasundaram, K., Ed.; EPFL Press: Lausanne, 2009.
(8) Schmidt-Mende, L.; Grätzel, M. *Thin Solid Films* **2006**, *500*, 296−301.
(9) Ding, I.-K.; Tétreault, N.; Brillet, J.; Hardin, B. E.; Smith, E.; Rosenthal, S.; Sauvage, F.; Grätzel, M.; Mcgehee, M. D. *Adv. Funct. Mater.* **2009**, *19*, 2431−2436.
(10) Melas-Kyriazi, J.; Ding, I.-K.; Marchioro, A.; Punzi, A.; Hardin, B. E.; Burkhard, G. F.; Tétreault, N.; Grätzel, M.; Moser, J.-E.; McGehee, M. D. *Adv. Energy Mater.* **2011**, *1*, 407−414.
(11) Tétreault, N.; Horváth, E.; Moehl, T.; Brillet, J.; Smajda, R.; Bungener, S.; Cai, N.; Wang, P.; Zakeeruddin, S. M.; Forró, L.; Magrez, A.; Grätzel, M. *ACS Nano* **2010**, *4*, 7644−7650.
(12) Sommeling, P. M.; O'Regan, B. C.; Haswell, R.; Smit, H.; Bakker, N.; Smits, J.; Kroon, J.; Van Roosmalen, J. *J. Phys. Chem. B* **2006**, *110*, 19191−19197.
(13) O'Regan, B. C.; Durrant, J. R.; Sommeling, P. M.; Bakker, N. J. *J. Phys. Chem. C* **2007**, *111*, 14001−14010.
(14) Kambe, S.; Nakade, S.; Wada, Y.; Kitamura, T.; Yanagida, S. *J. Mater. Chem.* **2002**, *12*, 723−728.
(15) Wang, P.; Klein, C.; Humphry-Baker, R.; Zakeeruddin, S. M.; Grätzel, M. *J. Am. Chem. Soc.* **2005**, *127*, 808−809.
(16) Teuscher, J. Ph.D. Thesis No. 4731, EPF Lausanne, 2010.
(17) Tachibana, Y.; Moser, J.-E.; Grätzel, M.; Klug, D.; Durrant, J. R. *J. Phys. Chem.* **1996**, *100*, 20056−20062.
(18) Kallioinen, J.; Benkö, G.; Myllyperkio, P.; Khriachtchev, L.; Skarman, B.; Wallenberg, R.; Tuomikoski, M.; Korppi-Tommola, J.; Sundström, V.; Yartsev, A. P. *J. Phys. Chem. B* **2004**, *108*, 6365−6373.
(19) Wenger, B.; Grätzel, M.; Moser, J.-E. *J. Am. Chem. Soc.* **2005**, *127*, 12150−12151.
(20) Moser, J.-E. In *Dye-Sensitized Solar Cells*; Kalyanasundaram, K., Ed.; EPFL Press: Lausanne, 2009.

(21) Tiwana, P.; Parkinson, P.; Johnston, M. B.; Snaith, H. J.; Herz, L. M. *J. Phys. Chem. C* **2010**, *114*, 1365−1371.
(22) Bach, U.; Tachibana, Y.; Moser, J.-E.; Haque, S. A.; Durrant, J. R.; Grätzel, M.; Klug, D. *J. Am. Chem. Soc.* **1999**, *121*, 7445−7446.
(23) Bonhôte, P.; Gogniat, E.; Tingry, S.; Barbé, C.; Vlachopoulos, N.; Lenzmann, F.; Comte, P.; Grätzel, M. *J. Phys. Chem. B* **1998**, *102*, 1498−1507.
(24) Ardo, S.; Meyer, G. J. *J. Am. Chem. Soc.* **2011**, *133*, 15384−15396.
(25) Snaith, H. J.; Humphry-Baker, R.; Chen, P.; Cesar, I.; Zakeeruddin, S. M.; Grätzel, M. *Nanotechnology* **2008**, *19*, 424003.
(26) Marchioro, A. Unpublished results.
(27) Laskova, B.; Zukalova, M.; Kavan, L.; Chou, A.; Liska, P.; Wei, Z.; Bin, L.; Kubat, P.; Ghadiri, E.; Moser, J.-E.; Grätzel, M. *J. Solid State Electrochem.* **2012**, *16*, 2993−3001.

Effect of post-treatment of titania mesoscopic films by $TiCl_4$ in solid-state dye-sensitized solar cells: A time-resolved spectroscopy study

*Arianna Marchioro,[a,b] Amalie Dualeh,[b] Angela Punzi,[a †] Michael Grätzel,[b] and Jacques-E. Moser [a] **

[a] Photochemical Dynamics Group and [b] Laboratory for Photonics and Interfaces,

Institute of Chemical Sciences and Engineering,

École Polytechnique Fédérale de Lausanne, CH-1015 Lausanne, Switzerland

SUPPLEMENTARY INFORMATION

Femtosecond Transient Absorption (TA) data treatment

The procedure for the fitting of the femtosecond TA signals is described herein. Electron injection was fitted with a model described elsewhere,[1,2] using the convolution of one Gaussian with two exponentials, the second exponential being fixed (τ = 10μs). For hole injection, a specific model was derived, allowing a correct description of the TAS signals by isolating the contribution of the dye regeneration from the electron injection, as in presence of spiro-OMeTAD these two processes occur on a very similar timescale. Furthermore, as small differences in the kinetics of electron injection were noticed in the $TiCl_4$ treated samples with respect to non-treated samples, this model also accounts for this factor.

The probe wavelength, 840 nm, was chosen in order to observe the oxidized state of the dye with little contribution from the excited state.[2-4] However this contribution cannot be totally neglected and thus the extinction coefficient of the excited state will be discussed further on. Past work on the kinetics of hole injection[5] probed the rise of the oxidized state of the HTM. In this work, we decided to probe the rise and decrease of the oxidized dye, in order to take into account any eventual dye that would not be in contact with the HTM and thus, would not inject its hole. This could not be probed by looking at the rise of the oxidized state of the HTM. Ideally, no contribution for the HTM oxidized state is desired in order to observe the sole contribution of the oxidized dye. However, in the spectral region of oxidized dye absorption, this requirement could not be fulfilled and the data treatment must take into account a minimal contribution for the oxidized state of the HTM. Additionally, the absorption of the electrons in the same spectral region has to be addressed as well. This model did not address the issue of reductive quenching of the excited state of the dye by the HTM. Further studies will be conducted to determine the impact of this process on the overall kinetics.

The extinction coefficients of all the species present at 840 nm were determined. Z907 extinction coefficient was extracted by nanosecond flash photolysis experiments of Z907/TiO_2 samples, covered with an inert solvent, where the amplitude of the signal from oxidized dye at 840 nm was compared to the amplitude of the bleaching signal from the ground-state species. In the microsecond timescale of the experiment, no contribution from the excited state of the dye was expected and thus the extinction coefficient corresponds to species present after electron injection. By taking the extinction coefficient of the ground state species reported at 526 nm (ε_S = $1.2 \cdot 10^4$ M^{-1} cm^{-1}),[6] we could calculate a value of

$6.7 \cdot 10^3$ M^{-1} cm^{-1} corresponding to the extinction coefficient of the oxidized species plus the corresponding free electrons in the conduction band that have broad absorption spectra in the IR. From the same flash photolysis measurements at longer wavelengths and based on the literature,[7,8] we could estimate this value for the electrons as being approximately $\varepsilon_{e^-} = 1.3 \cdot 10^3$ M^{-1} cm^{-1}, leading to a value of $\varepsilon_{S+} = 5.4 \cdot 10^3$ M^{-1} cm^{-1} for the oxidized species alone. We further assume for the purpose of this analysis that the extinction coefficient of the electrons is independent of the concentration. This is not the case for strong accumulation conditions,[9] but the laser intensities used in the femtosecond study should not exceed 8 electrons/TiO_2 nanoparticle.

The extinction coefficient of the first oxidized form of spiro-OMeTAD, formed by regeneration of the oxidized dye, is also weakly absorbing at this wavelength, with an extinction coefficient of $\varepsilon_{D+} = 8.5 \cdot 10^2$ M^{-1} cm^{-1} as determined by NIR absorption of the chemically oxidized form, in agreement with previously measured values.[10,11] To the best of our knowledge, the extinction coefficient of the excited state (denoted ε_{S^*}) was not reported clearly in the literature. For the purpose of this quantitative model, we thus tried to extract an approximate value for the extinction coefficient of the excited state species. From data published in Tachibana's thesis and previous reports,[3,12] the relative amplitude of the excited state with respect to the signal of the oxidized species and the electrons is 27% of a signal constituted by oxidized state and electrons, i.e. an absorption coefficient of roughly $\varepsilon_{S^*} = 2.2 \cdot 10^3$ M^{-1} cm^{-1}.

Hence, on a total signal of oxidized dye S^+, excited state S*, electrons e- and oxidized HTM D^+ (ε_{tot} = 6700 + 2200 + 1300 + 850 = 11050 M^{-1} cm^{-1}), we have 60% contribution from the oxidized state, 20 % contribution from the excited state, 12% for the electrons and 8% coming from the oxidized HTM. These values will allow a correct weighting of the different contributions in the signal.

As the overall signal contains more than one contribution, it was necessary to separate the temporal evolution of each of these contributions. For this purpose, differential equations were used to describe the temporal evolution of the species. All the subpicosecond processes and the instrument response function were not taken into account in the kinetic model and considered as a step function, as the processes of interest were much slower.

After electron injection, the following process is hole injection into the HTM. A two-exponential process has been observed and previously described by Bach et al.,[5] and ascribed to a kinetic inhomogeneity, i.e. different types of populations. In our model, we consider a first type of population (A) that represents the oxidized dye molecules in close contact with the HTM; the rate constant for hole injection will be named k_A. A second type of population (B), represents the oxidized dye molecules at longer distances from the HTM, thus subjected to hole hopping to transfer their hole.[13] We made the assumption that statistically these distances will average giving rise to a unique rate constant, namely k_B. The ground state species, denoted S, can give rise after injection to either S_A^+ or S_B^+.

Considering the following reactions:

$$S^* \rightarrow S^+_{A,B} + e^-_{CB} \quad (1)$$

$$S^* \xrightarrow{k_1} S^+_A + e^-_{CB} \quad (2)$$

$$S^* \xrightarrow{k_1} S^+_B + e^-_{CB} \quad (3)$$

Eq. (1) describes the instantaneous rise within the laser pulse that is completed at time t=0. Eq. (2) and (3) take into account the slower injection part respectively for A and B populations. The time constant of this process, k_1, can readily be extracted from fitting a reference of Z907/TiO_2 and inert solvent. The time constant k_1 remains the same for both A and B populations as the electron injection is not related with the type of dye (in contact or not) with the HTM.

The regeneration of the different types of dye populations by HTM is given by the rate constants k_a and k_b in (4) and (5):

$$S^+_A + D \xrightarrow{k_A} S_A + D^+ \quad (4)$$

$$S^+_B + D \xrightarrow{k_B} S_B + D^+ \quad (5)$$

Thus the temporal evolution of the species can then be described by the following equations:

$$\frac{dS^*}{dt} = -2k_1 S^* \quad (6)$$

$$\frac{dS^+_A}{dt} = k_1 S^* - k_A S^+_A \quad (7)$$

$$\frac{dS_B^+}{dt} = k_1 S^* - k_B S_B^+ \tag{8}$$

$$\frac{dD^+}{dt} = k_A S_A^+ + k_B S_B^+ \tag{9}$$

with $S_A^+(t)$, $S_B^+(t)$ being the concentrations of the oxidized dye, respectively for populations A and B, and $D^+(t)$ being the concentration of the oxidized HTM. The initial conditions are $S^*(t=0) = S_0^*$, $S_A^+(t=0) = S_{A,0}^+$, $S_B^+(t=0) = S_{B,0}^+$ and $D^+(t=0) = D_0^+ = 0$.

The temporal evolution of the electrons must also be considered, and once they are formed, on the timescale of interest, we can consider that their concentration remains constant (recombination processes are much slower).

$$\frac{de^-}{dt} = -\frac{dS^*}{dt} = +2k_1 S^* \tag{10}$$

with $e_0^- = S_{A,0}^+ + S_{B,0}^+$. The system of differential equations (6),(7),(8),(9) and (10) can be solved in Mathematica (v.8.0.4.0).

Once the temporal evolution of the concentrations is found, the transient absorption signal (the change in absorbance with and without laser pulse) can be described by weighting each concentration with the corresponding *relative* extinction coefficient, following the Beer Lambert law:

$$\Delta A = A_{pump} - A_{no\,pump} = \sum_i \varepsilon_i \cdot c_i(t)_{pump} - \sum_i \varepsilon_i \cdot c_i(t)_{no\,pump} \tag{11}$$

As at this wavelength, the ground state species do not absorb, the second term of eq. (11) is zero and the overall equation is:

$$
\begin{aligned}
&\Delta A = \mathrm{e}^{-2k_1 t}\varepsilon_{S^*}S_0^* + \varepsilon_{electrons}(S_0^* - \mathrm{e}^{-2k_1 t}S_0^*) + \varepsilon_{electrons}(S_{A,0}^+ + S_{B,0}^+) \\
&+\frac{1}{(2k_1 - k_A)(2k_1 - k_B)}\mathrm{e}^{-2k_1 t - k_A t - k_B t}\varepsilon_{D^+}\cdot(-2\mathrm{e}^{2k_1 t + k_A t}k_1^2 S_0^* - 2\mathrm{e}^{2k_1 t + k_B t}k_1^2 S_0^* \\
&+4\mathrm{e}^{2k_1 t + k_A t + k_B t}k_1^2 S_0^* + \mathrm{e}^{2k_1 t + k_A t}k_1 k_A S_0^* + \mathrm{e}^{k_A t + k_B t}k_1 k_A S_0^* - 2\mathrm{e}^{2k_1 t + k_A t + k_B t}k_1 k_A S_0^* \\
&+\mathrm{e}^{2k_1 t + k_B t}k_1 k_B S_0^* + \mathrm{e}^{k_A t + k_B t}k_1 k_B S_0^* - 2\mathrm{e}^{2k_1 t + k_A t + k_B t}k_1 k_B S_0^* - \mathrm{e}^{k_A t + k_B t}k_A k_B S_0^* \\
&+\mathrm{e}^{2k_1 t + k_A t + k_B t}k_A k_B S_0^* - 4\mathrm{e}^{2k_1 t + k_B t}k_1^2 S_{A,0} + 4\mathrm{e}^{2k_1 t + k_A t + k_B t}k_1^2 S_{A,0} + 2\mathrm{e}^{2k_1 t + k_B t}k_1 k_A S_{A,0} \\
&-2\mathrm{e}^{2k_1 t + k_A t + k_B t}k_1 k_A S_{0,A} + 2\mathrm{e}^{2k_1 t + k_B t}k_1 k_B S_{A,0} - 2\mathrm{e}^{2k_1 t + k_A t + k_B t}k_1 k_B S_{A,0} \\
&-\mathrm{e}^{2k_1 t + k_B t}k_A k_B S_{A,0} + \mathrm{e}^{2k_1 t + k_A t + k_B t}k_A k_B S_{A,0} - 4\mathrm{e}^{2k_1 t + k_A t}k_1^2 S_{B,0} + 4\mathrm{e}^{2k_1 t + k_A t + k_B t}k_1^2 S_{B,0} \\
&+2\mathrm{e}^{2k_1 t + k_A t}k_1 k_A S_{B,0} - 2\mathrm{e}^{2k_1 t + k_A t + k_B t}k_1 k_A S_{B,0} + 2\mathrm{e}^{2k_1 t + k_A t}k_1 k_B S_{B,0} \\
&-2\mathrm{e}^{2k_1 t + k_A t + k_B t}k_1 k_B S_{B,0} - \mathrm{e}^{2k_1 t + k_A t}k_A k_B S_{B,0} + \mathrm{e}^{2k_1 t + k_A t + k_B t}k_A k_B S_{B,0}) \\
&+\varepsilon_{S^+}(-\frac{\mathrm{e}^{-2k_1 t - k_A t}(-\mathrm{e}^{2k_1 t}k_1 S_0^* + \mathrm{e}^{k_A t}k_1 S_0^* - 2\mathrm{e}^{2k_1 t}k_1 S_{A,0} + \mathrm{e}^{2k_1 t}k_A S_{A,0})}{2k_1 - k_A} \\
&-\frac{\mathrm{e}^{-2k_1 t - k_B t}(-\mathrm{e}^{2k_1 t}k_1 S_0^* + \mathrm{e}^{k_B t}k_1 S_0^* - 2\mathrm{e}^{2k_1 t}k_1 S_{B,0} + \mathrm{e}^{2k_1 t}k_B S_{B,0})}{2k_1 - k_B})
\end{aligned}
\tag{12}
$$

where the extinction coefficients are listed above.

Eq. (12) can be used as a fit function in Igor (v. 6.00) with the corresponding initial guesses on $S_{A,0}{}^+$ and $S_{B,0}{}^+$ and the relative extinction coefficients as fixed parameters. As previously mentioned, the subpicosecond processes and the instrument response function were taken as a step function in this analysis, as the processes of interest were much slower, thus the fits start at t = 1 ps. S_0^* and k_1 were both estimated from the reference of Z907/TiO_2 with inert solvent and taken as fixed parameters. k_b, the slowest exponential, needed to be sometimes fixed (usually 30 ns). Thus on a total of ten parameters, seven are fixed or constrained.

Estimation of the S_0* parameter

The initial concentration of excited state can be extracted from a fitting a reference of Z907/TiO_2, in absence of spiro-OMeTAD. It is calculated considering only the growth after the subicosecond, ultrarapid injection. The amplitude of this slow part, denoted ΔA_{slow} and shown in fig.1, is given by the following equation:

$$\Delta A_{slow} = \Delta A_{S_f^+} + \Delta A_{e_f^-} = \varepsilon_{S^+} S_f^+ + \varepsilon_{e^-} e_f^- \tag{13}$$

and $S_0^* = S_f^+ = e_f^-$. (fig. 1), where S_f^+ is the final concentration of oxidized dye and e_f^- the final concentration of electrons, corresponding to the species produced in the slow part.

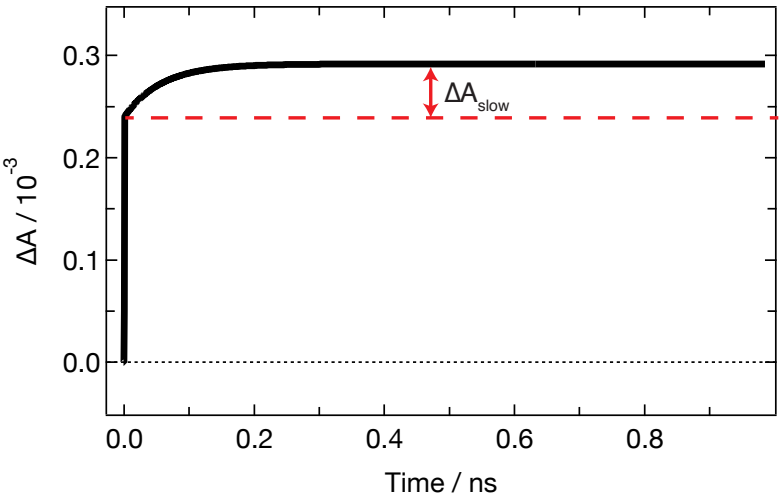

Figure 1. *Scheme showing the amplitude of the slow part ΔA_{slow}*

Thus:

$$S_0^* = S_f^+ = \frac{\Delta A_{S_f^+}}{\varepsilon_{S^+}} = \frac{\Delta A_{slow} - \Delta A_{e_f^-}}{\varepsilon_{S^+}} = \frac{\Delta A_{slow} - \varepsilon_{e_f^-} e_{e_f^-}}{\varepsilon_{S^+}} = \frac{\Delta A_{slow} - \varepsilon_{e_f^-} S_0^*}{\varepsilon_{S^+}} \tag{14}$$

$$S_0^* = \frac{\Delta A_{slow}}{(\varepsilon_{S^+} + \varepsilon_{e_f^-})} \tag{15}$$

In this case, the only species present are S^+, S^* and e^-. The relative extinction coefficients, for the excited state absorption, the oxidized state and the electrons, are 66%, 21% and 13%. The initial excited state concentration becomes:

$$S_0^* = \frac{\Delta A_{slow}}{(0.66 + 0.13)} \tag{16}$$

This allows an estimation of the initial concentration of excited state from the reference and thus can be put as a constrained parameter in the fit equation (12).

Residuals of the fits

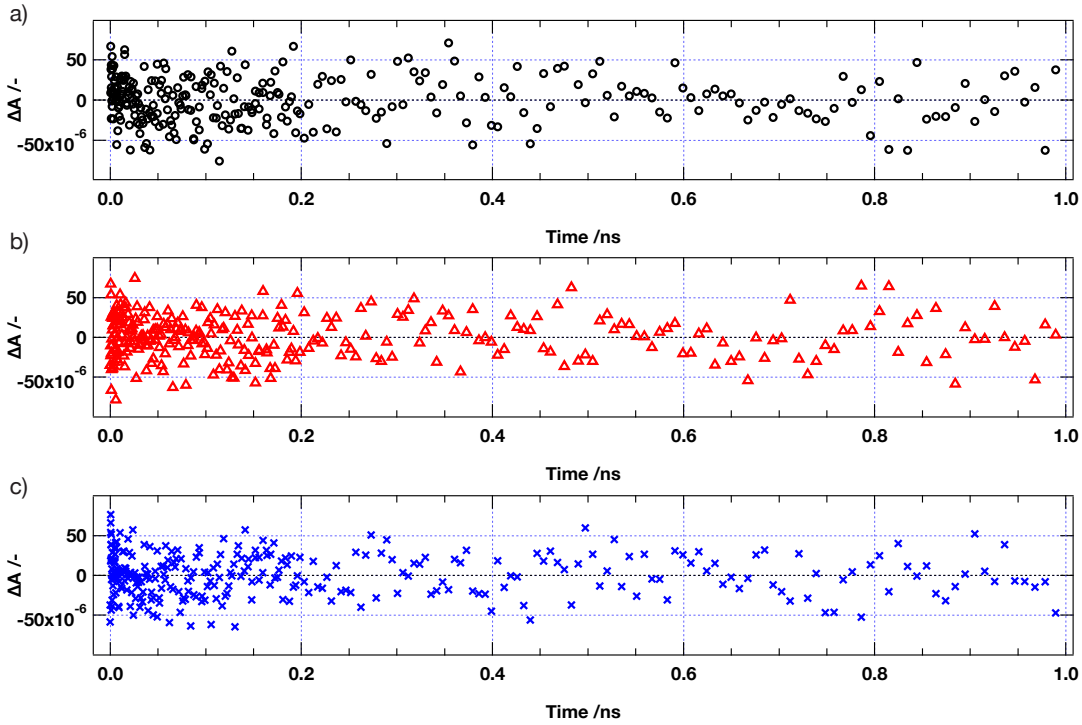

Figure 2. *Residues of the fits of hole injection spectra monitored at 840 nm followed by excitation at 590 nm on a) Z907 + spiro-OMeTAD/non-treated TiO_2*

(black dots) , b) on Z907 + spiro-OMeTAD/70°C treated TiO_2 (red triangles) and c) on Z907 + spiro-OMeTAD/RT treated TiO_2 (blue crosses).

Absorption Spectra

The absorption spectra of the films with and without HTM are reported here. The UV-vis-near IR spectrum was measured with a Lambda 950 spectrophotometer (Perkin-Elmer) equipped with a 60 mm integrating sphere (LabSphere). A total transmission spectrum was measured for the films measuring between 2 and 2.5um. The RT treatment and the 70°C treatment being very similar, only the results for the 70°C treatment are presented here.

Absorption spectra for Z907/TiO_2. The absorption spectra derived from the total transmission of Z907 adsorbed on the 70°C treatment film and the non-treated film are shown in fig. 3. They both show a maximum at 525 nm, accordingly to the values reported in the literature. [6]

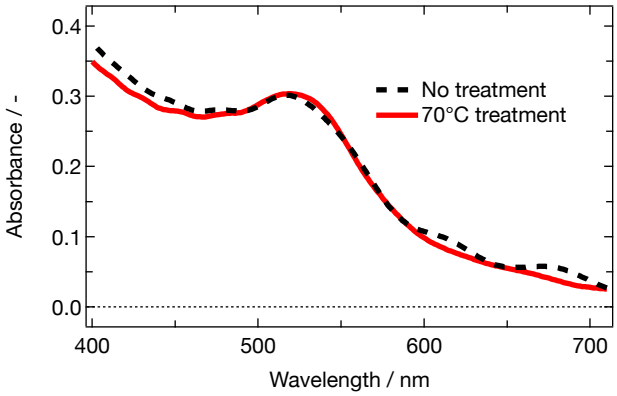

Figure 3. *Absorbance spectra of Z907/TiO_2 non-treated film (dashed black line) and 70°C treated film (red plain line).*

Absorption spectra for desorbed Z907. In order to quantitatively estimate the difference in dye loading on a treated and non-treated film, dye desorption experiments, as already described by Sommeling et al.[14] were performed on the same films used for the integrating sphere measurements. First, the thickness of the films was measured with profilometer (Alpha-Step 500 profilometer, KLA-Tencor) as shown in table 1. The area of all the films was identical.

Table 1. *Thickness of the non-treated and 70°C treated TiO_2 films before dyeing*

Sample	Average thickness (um)
No treatment	1.96
70°C treatment	2.47

Then, after usual dyeing procedure, a solution (1:1) NaOH 0.1M/H_20 was prepared in order to desorb the dye from the TiO_2 surface. The solutions were then measured with the standard detector of the Lambda 950 spectrophotometer. The spectra were slightly blue-shifted, indicating a partial deprotonation of the dye. To obtain the exact dye loading, the absorbance of the desorbed solutions was divided by the average film thickness (fig. 4). As expected, the difference was small, in the order of 4%, this confirming the values reported in Sommeling's paper.

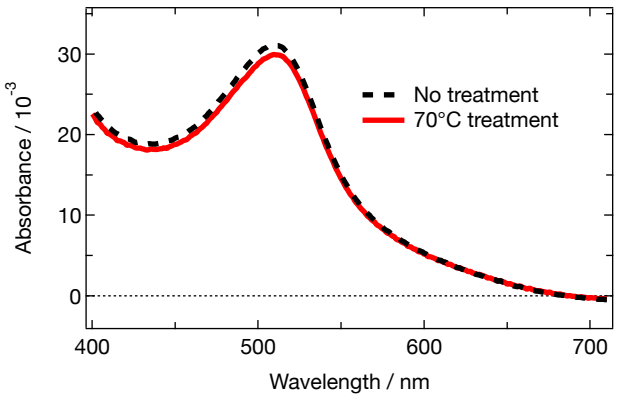

Figure 4. *Absorbance of a solution of desorbed Z907 from non-treated film (dashed black line) and 70°C treated film (red plain line), divided by the corresponding film thickness.*

Absorption of Z907+spiro-OMeTAD/TiO_2. The spectra of the samples with spiro-OMeTAD shows the same absorption peak for the dye as well as a supplementary feature at 400 nm – indicative of presence of unoxidized spiro-OMeTAD (fig. 5).

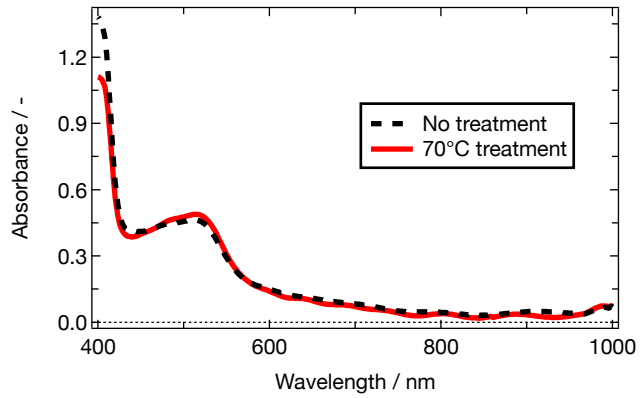

Figure 5. *Absorbance spectra of Z907+spiro-OMeTAD/TiO_2 non-treated film (dashed black line) and 70°C treated film (red plain line).*

SEM pictures

A difference between the TiO_2 underlayers with and without $TiCl_4$ treatment can be observed on the SEM pictures. When compared to a non-treated underlayer (fig. 6a), the 70°C treatment (fig. 6b) shows formation of a structured layer over the TiO_2 sprayed layer,

that appears to be conformal. With RT treatment (fig. 6c), the formation of an additional layer includes the nucleation of small islands (white dots) on the compact TiO_2 layer. In both cases, more material is deposited over the substrate, inducing a change in the surface structure and properties that, in the case of the mesoporous TiO_2 structure, will most likely modify the contact between TiO_2 nanoparticles and the HTM.

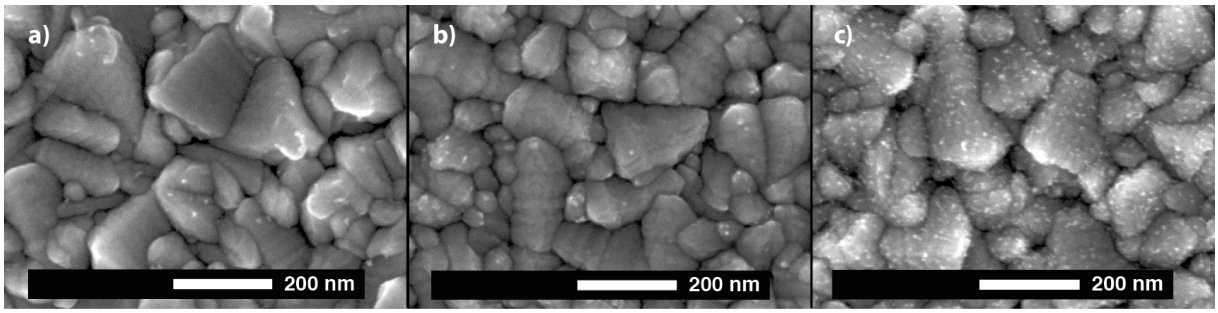

Figure 6. *SEM pictures of a) Non-treated TiO_2 underlayer, b) 70°C treated TiO_2 underlayer and c) RT treated TiO_2 underlayer.*

(1) Van Stokkum, H. I., *Global and target analysis of time-resolved spectra*, Lecture notes 'Troisième Cycle de la Physique en Suisse Romande', **2005**.
(2) Teuscher, J. *PhD Thesis n°4731,* EPF Lausanne*,* **2010**.
(3) Tachibana, Y., *PhD Thesis*, Imperial College London, **1999**.
(4) Kallioinen, J.; Benkö, G.; Sundström, V.; Korppi-Tommola, J.; Yartsev, A. P. *J. Phys. Chem. B* **2002**, *106*, 4396–4404.
(5) Bach, U.; Tachibana, Y.; Moser, J.-E.; Haque, S. A.; Durrant, J. R.; Grätzel, M.; Klug, D. *J. Am. Chem. Soc.* **1999**, *121*, 7445–7446.
(6) Nazeeruddin, M. K.; Zakeeruddin, S. M.; Humphry-Baker, R.; Jirousek, M.; Liska, P.; Vlachopoulos, N.; Shklover, V.; Fischer, C.-H.; Grätzel, M. *Inorganic Chemistry* **1999**, *38*, 6298–6305.
(7) Kay, A.; Humphry-Baker, R.; Grätzel, M. *J. Phys. Chem* **1994**, *98*, 952–959.
(8) Boschloo, G.; Fitzmaurice, D. *J. Phys. Chem. B* **1999**, *103*, 2228–2231.
(9) Boschloo, G.; Fitzmaurice, D. *J. Phys. Chem. B* **1999**, *103*, 7860–7868.
(10) Cappel, U.; Gibson, E.; Hagfeldt, A.; Boschloo, G. *J. Phys. Chem. C* **2009**, *113*, 6275–6281.
(11) Olson, C.; Veldman, D.; Bakker, K.; Lenzmann, F. *International Journal of Photoenergy* **2011**, *2011*, 1–11.
(12) Moser, J.-E.; Noukakis, D.; Bach, U.; Tachibana, Y.; Klug, D.; Durrant, J. R.; Humphry-Baker, R.; Grätzel, M. *J. Phys. Chem. B* **1998**, *102*, 3649–3650.
(13) Ardo, S.; Meyer, G. J. *J. Am. Chem. Soc.* **2011**, *133*, 15384–15396.
(14) Sommeling, P. M.; O'Regan, B. C.; Haswell, R.; Smit, H.; Bakker, N.; Smits, J.; Kroon, J.; Van Roosmalen, J. *J. Phys. Chem. B* **2006**, *110*, 19191–19197.